Sub-wavelength imaging at radio frequency

2006 J. Phys.: Condens. Matter 18 L315

(http://iopscience.iop.org/0953-8984/18/22/L06)

INSTITUTE OF PHYSICS PUBLISHING JOURNAL OF PHYSICS: CONDENSED MATTER

J. Phys.: Condens. Matter **18** (2006) L315–L321 doi:10.1088/0953-8984/18/22/L06

LETTER TO THE EDITOR

Sub-wavelength imaging at radio frequency

M C K Wiltshire[1,2], J B Pendry[2] and J V Hajnal[1]

[1] Imaging Sciences Department, Imperial College London, Hammersmith Hospital, London W12 0HS, UK
[2] The Blackett Laboratory, Imperial College London, London SW7 2AZ, UK

E-mail: michael.wiltshire@imperial.ac.uk

Received 29 March 2006
Published 19 May 2006
Online at stacks.iop.org/JPhysCM/18/L315

Abstract

A slab of material with a negative permeability can act as a super-lens for magnetic fields and generate images with a sub-wavelength resolution. We have constructed an effective medium using a metamaterial with negative permeability in the region of 24 MHz, and used this to form images in free space of radio frequency magnetic sources. Measurements of these images show that a resolution of approximately $\lambda/64$ has been achieved, consistent with both analytical and numerical predictions.

(Some figures in this article are in colour only in the electronic version)

Conventional optical systems cannot resolve features that are much smaller than the wavelength, λ, of the electromagnetic radiation being used [1], because their optical components act only on the phase of the radiation and so only focus the propagating field. However, it has recently been shown [2] that a material with a refractive index $n = -1$ allows both the propagating and the evanescent fields to be focused, so that sub-wavelength imaging can be achieved. An ideal slab of such material of thickness d should form an image in a plane $2d$ from the source with no loss of resolution. This was a controversial concept, which has now come to be accepted (see e.g. [3]) due in part to the use of metamaterials to provide the necessary negative index material.

Materials with negative refractive index do not occur in nature, but can be constructed artificially. By including conducting elements that exhibit the required electromagnetic response but are small compared to a wavelength, metamaterials can be made that have the desired permeability and permittivity [4–6]. Combinations of such materials have been shown experimentally to possess a negative refractive index [7, 8]. The first demonstration of sub-wavelength imaging by negative index material was made at microwave frequency using a transmission line geometry [9]. A region with negative index was sandwiched between two regions of conventional line, and produced an image of a point source with a linewidth of $\sim\lambda/3$.

However, it was also pointed out in [2] that when all relevant lengths are very much less than the wavelength, the electric and magnetic components of electromagnetic radiation are decoupled. In this very near field regime, therefore, an electric signal can be focused using a material with permittivity $\varepsilon = -1$, irrespective of its permeability. Metals have a negative permittivity below their plasma frequency, and experiments have recently been performed using very thin silver films to demonstrate images with sub-wavelength resolution, and a resolution of $\lambda/6$ was achieved [10–12].

A magnetic signal could likewise be focused in the very near field using material with permeability $\mu = -1$, but materials with this property are not found in nature, so this focusing has not yet been observed. However, metamaterials consisting of structured elements much smaller than λ allow us to construct materials with specified μ [6], and in particular with $\mu = -1$. Moreover, by working at radio frequency (RF), the requirements that both the material elements and the measurement distance should be much smaller than a wavelength are readily satisfied. Therefore, we have constructed such a material that operates at RF, and used it to demonstrate imaging with a resolution of $\lambda/64$.

The metamaterial design used here is the 'Swiss Roll' [6], and consists of several turns of a copper/kapton laminate wound onto a central former. This structure provides a resonant response to an incident magnetic field, so that an ensemble of such elements can be described as having a complex effective permeability of the form [6, 13]

$$\mu(f) = 1 - \frac{F}{\left(1 - \frac{f_0^2}{f^2}\right) + \mathrm{i}\frac{\gamma}{f}}. \tag{1}$$

Here, f_0 is the resonant frequency, F is the packing density, γ is a damping term and $\mathrm{i} = \sqrt{-1}$. The real and imaginary parts of the permeability are denoted by μ' and μ'' respectively. The 'Swiss Roll' structure is very active magnetically: peak permeabilities in excess of 30 can be achieved, and the bandwidth of the negative permeability regime can extend to 40% of the resonant frequency [13]. It is therefore a medium that is well-suited to investigating sub-wavelength imaging in the very near field, because the frequency at which $\mu' = -1$ is well removed from the resonance frequency, and hence μ'' is small. In the present case, we have used 11 turns of Espanex® SC-18-12-00-FR wound onto a 10 mm diameter polymer mandrel to give rolls with a resonant frequency of 21.5 MHz, and a uniaxial permeability [14, 15] as shown in figure 1(a). Each roll was initially 50 mm long, but carried an additional tuning sleeve that extended by a further 10 mm to ensure that all rolls could be the same length and be tuned to the same frequency within 0.1 MHz [13].

It is important to distinguish between focusing [2] and the endoscope behaviour that we reported previously [13]. When a metamaterial acts as a focusing element, as in the present case, an object field distribution in free space is transformed to an image field distribution, also in free space, by the action of the metamaterial. The endoscope, on the other hand, transfers the field distribution on one side of the metamaterial unchanged to the other side: there is no focusing action—the material acts as a face-plate, not a lens.

To observe these focusing effects [2], the material should be isotropic; anisotropic materials behave in a very different way [13] as has also been shown in studies of the anisotropic electrical plasma [16], although focusing has been reported [17] using anisotropic transmission line material. However, if we confine our attention to the (x, z) plane (where z is the direction of propagation and x is a transverse direction) by making the components in the experiment extend uniformly in the y-direction, it is possible to work with a two-dimensional (2D) isotropic material, so that $\mu_x = \mu_z = \mu(\omega)$ and $\mu_y = 1$. Such material can be constructed by assembling the rolls in a 2D log-pile, with alternate layers being stacked axially and transversely, as shown schematically in figure 1(b). Our studies [15] have shown

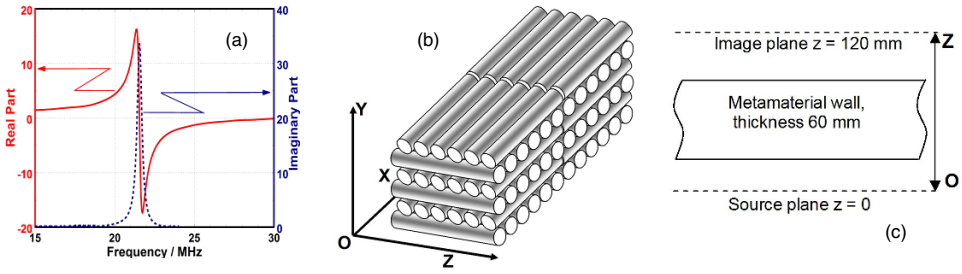

Figure 1. (a) The measured permeability for a single 'Swiss Roll', showing both the real part (full line (red) and left axis) and the imaginary part (dotted line (blue) and right axis), (b) a schematic diagram showing the packing of the rolls for the 2D log-pile structure, and (c) a schematic diagram of the set-up used in both the experiment and the simulation: the magnetic line sources are placed 20 mm behind the metamaterial slab of thickness 60 mm; the image plane is 120 mm from the sources.

that a rich set of surface resonances appears for frequencies where μ' is negative, and to prevent these from obscuring the focusing effects that we seek, it is desirable to make the sample as long as possible. Accordingly, 300 rolls were stacked in a log-pile, with the individual rolls and layers being suitably spaced so as to obtain $\mu_x = \mu_z$. This provided a slab of material that was 385 mm wide (OX), 60 mm thick (OZ) and 90 mm high (OY), so that the central unit layer was surrounded by $1\frac{1}{2}$ layers in an approximation of an extended medium.

The magnetic field sources each consisted of two antiparallel wires that served to generate a line of magnetic flux, and these were placed 20 mm behind the slab. A long narrow rectangular loop that spanned the height of the central unit layer was used to measure the average longitudinal component of the magnetic field, H_z, and was scanned in the output space using a custom-built translation table. Measurements of H_z were made on a 5 mm spatial grid, using an Agilent 8753ES network analyser to record the field at 401 frequency points between 15 and 35 MHz.

Two sets of measurements were performed. For measurements using a single source, this was placed on the centre line of the metamaterial slab; for measurements with two sources, these were placed symmetrically about the centre line. Because the scanning range of the translation table was limited to 300 mm, the maximum separation of the sources was restricted so that data could be taken on either side of both sources. Accordingly, scan data were collected for source separations of 100, 120 and 140 mm.

The resolution enhancement, R, that can be achieved with a negative index slab was calculated analytically in [18–20], where it was shown that the limit of resolution, Δ, is determined by the loss in the material, which here is μ'', and by the length of the sample, d, to be

$$R = \frac{\lambda}{\Delta} = -\frac{1}{2\pi}\ln(\mu''/2)\frac{\lambda}{d} \qquad \text{or} \qquad \Delta = \frac{2\pi d}{|\ln(\mu''/2)|}. \tag{2}$$

Using the data in figure 1(a), we estimate the parameters in (1) for a single roll to be $f_0 = 21.55$ MHz, $\gamma = 0.36$ MHz, and $F = 0.56$ [15]. When the rolls are assembled into a prism, the filling factor is reduced, in the present case by a factor of $\pi/4$ to $F = 0.44$. Using these values, we obtain $\mu'' = 0.14$ when $\mu' = -1$, so that $\Delta \approx 140$ mm and $R \approx 90$. It should be noted that Δ is independent of the wavelength of operation, emphasizing the advantage of working at long wavelength in the RF, to minimize the impact of loss in the metamaterial on the resolution enhancement.

As a further check that the material would be able to show sub-wavelength imaging, we carried out a numerical simulation using MicroWave Studio® [21]. The proposed experimental set-up was modelled as shown in figure 1(c). The sample was a slab of material, 60 mm thick and 400 mm long, having a 2D isotropic permeability with a Lorentzian dispersion (as observed experimentally). In-built constraints in the software prevented us from using the parameters derived from those given above (i.e. $\mu_s = 1, \mu_\infty = (1 - F) = 0.56$); instead, we had to use an approximation to the permeability function, retaining the correct resonant frequency and damping, but using a static permeability $\mu_s = 1.54$ and $\mu_\infty = 1$, which has the effect of reducing the negative permeability region slightly, so that although μ has the same functional form in both cases, it is rather less negative in the model. With these values, we found $\mu' = -1$ at 24.28 MHz; then $\mu'' = 0.14$, in good agreement with the value derived from the measurements. The simulation was run with two sources placed 100 mm apart, and the field pattern in the image space was calculated, first with no metamaterial present to give a reference and then with the material slab in place. When the metamaterial was present, the field amplitude in the image plane was increased by a factor of about 15, and there was a pronounced double peak structure in the distribution confirming that sub-wavelength resolution should be achievable.

The experimental data consist of measurements of H_z as a function of frequency at each grid point in the output space. These have been analysed to generate maps of the spatial field distribution at each frequency. However, although we have given an estimate above, the permeability of the experimental structure is not precisely known, so the frequency at which $\mu' = -1$ is uncertain. Moreover, it has been shown [20] that deviations from the ideal values of μ significantly reduce the performance of the material. Accordingly, it was essential to determine the correct frequency, and we have used our simulated results to guide the interpretation of the experimental data.

The simulation was run for source separations between 80 and 140 mm apart to match the experimental cases, and the field pattern in the (x, z) plane of the image space was calculated as a function of frequency. From these data, we extracted the field in the theoretical image plane, at $z = 120$ mm, and generated a plot of the simulated field magnitude, $|H_z|$, as a function of frequency and position in the image plane, similar to that shown in [22], for each of the source separations. The case when the separation is 100 mm is shown in figure 2(a), with the frequency at which $\mu' = -1$ being marked with a dashed line.

There are several characteristic features of this plot. First, there are two regions of high intensity, separated by ∼100 mm, which correspond to the images of the sources. These occur

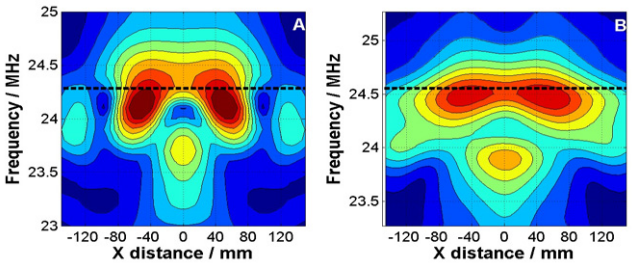

Figure 2. Maps of the field magnitude transmitted through the metamaterial as a function of frequency and position in the image plane, obtained from two sources spaced 100 mm apart. (A) The simulated distribution; the dashed line shows the frequency for which $\mu' = -1$. (B) The measured distribution which shows a similar structure at a slightly higher frequency; the dashed line is at 24.55 MHz, identifying where $\mu' = -1$.

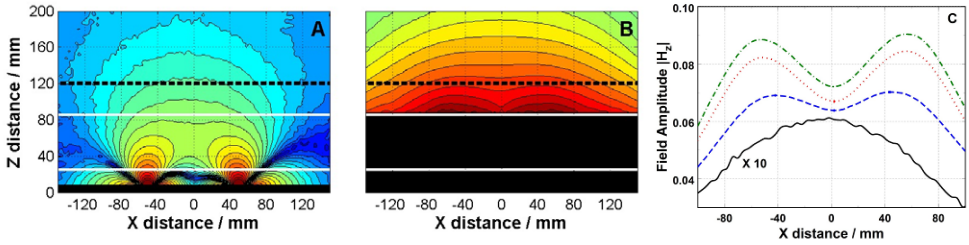

Figure 3. Measured distributions of H_z field intensity (dB) at 24.55 MHz. (A) From two sources spaced 100 mm apart in free space; (B) as (A) but with the metamaterial slab in place. In these frames, the position of the metamaterial is indicated by the thin white line, and the image plane by the dashed black line. (C) The variation of the field amplitude in the image plane $z = 120$ mm without the metamaterial (full black line, $\times 10$), and with the metamaterial when the sources are spaced 100 mm (dashed blue line), 120 mm (dotted red line) and 140 mm (dash–dot green line) apart.

at the frequency when $\mu' = -1$ and extend to lower frequency. At lower frequency, the field is confined to the central region only. It should be noted, however, that the resonant frequency of this system is 21.55 MHz, so that the permeability is strongly negative throughout the entire range of figure 2.

The experimental data were analysed in a similar way, and the equivalent plot for the measured data is shown in figure 2(b); we can see that there is a striking similarity between the measured and simulated plots. By noting that the $\mu' = -1$ frequency lies just above the high intensity regions in the simulation (figure 2(a)), we identified 24.55 MHz, which similarly lies just above the equivalent high intensity regions in figure 2(b), as the frequency at which $\mu' = -1$ in the experimental system.

The experimental data were then re-plotted to show the spatial distribution in the image space at 24.55 MHz. This is shown in figure 3. Here, figure 3(a) shows the distribution of $|H_z|$ arising just from the two sources, spaced 100 mm apart. We note that there is no discernible structure at 120 mm from the source plane. When the slab of metamaterial is introduced in the position indicated in figures 3(a) and (b), the fields in the image plane are enhanced by a factor of $\sim$15, and significant structure is obtained. Near the surface of the metamaterial, there are strong fields with rapid spatial variation—note that the intensity scale is the same in both frames. In the image plane, indicated by a dashed line in figures 3(a) and (b), distinct modulation can be seen. Plotting the field magnitude as a function of position in the image plane shows two peaks (figure 3(c)). As the source separation is increased, the weakly modulated peaks observed at the lowest value of 100 mm are split into two distinct peaks with appropriate spacing and increasing contrast. This confirms that the structure in the image plane does indeed arise from imaging the sources.

An analytical expression for the transfer function of a slab of negative index material has been given by Smith *et al* [20], who showed results for a slab with $d/\lambda = 0.1$, which gave a maximum resolution of $k/k_0 \approx 10$. In the present case, we have $d/\lambda = 0.005$, so our system should be more tolerant to loss, and still achieve higher resolution. We have used the formula of [20] to calculate the transfer function for our case using the predicted value of $\mu'' = 0.14$. This is shown as the dashed curve in figure 4.

To measure the transfer function, we used a single source, and carried out a line scan in the image plane. These data were then Fourier transformed to generate the transmission as a function of wavevector, and the resulting points were also plotted in figure 4. It is clear that the actual value of μ'' is rather larger than that estimated from measurements of a single

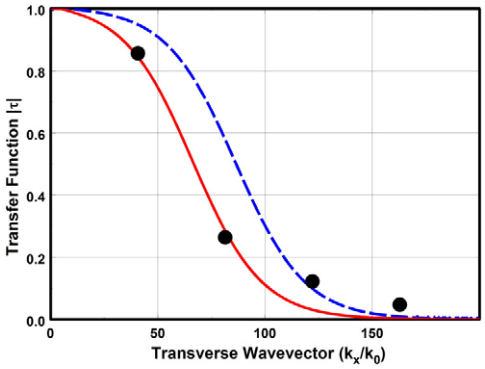

Figure 4. Measured (points) and calculated (lines) transfer function for a 60 mm slab of metamaterial with $\mu' = -1$ at 24.55 MHz: dashed (blue) line $\mu'' = 0.14$, full (red) line $\mu'' = 0.26$.

element. The least-squares fitted value is $\mu'' = 0.26$, and the transfer function for this value is plotted as the full line in figure 4. To estimate the resolution enhancement achieved, we transform this transfer function to real space and apply the Rayleigh criterion, that the ratio of the intensity mid-way between two just-resolved peaks to the maximum intensity is 81%. This shows that the two sources should be resolved when they are 190 mm apart, a resolution of $\sim\lambda/64$, although the measurements actually display a rather higher resolution, as indicated by the high spatial frequency tail in figure 4.

In conclusion, we have exploited the fact that at 25 MHz metamaterials can readily be constructed with individual elements that are much smaller than the wavelength ($\sim$12 m), so geometries in which all processes therefore take place in the very near field are simple to achieve. By using a suitable magnetic metamaterial we have demonstrated that sub-wavelength imaging with a resolution of $\lambda/64$ can be achieved when $\mu' = -1$. This is limited by losses, so that with the improved materials that we are currently developing, even smaller separations might be resolved.

MCKW is supported by the EC Information Societies Technology (IST) programme Development and Analysis of Left-Handed Materials (DALHM), Project number: IST-2001-35511. JVH thanks Philips Medical Systems for research grant support.

References

[1] Born M and Wolf E 1999 *Principles of Optics* 7th edn (Cambridge: Cambridge University Press) pp 543–53
[2] Pendry J B 2000 *Phys. Rev. Lett.* **85** 3966
[3] Smith D R, Pendry J B and Wiltshire M C K 2004 *Science* **305** 788
[4] Pendry J B, Holden A J, Stewart W J and Youngs I 1996 *Phys. Rev. Lett.* **76** 4773
[5] Pendry J B, Holden A J, Robbins D J and Stewart W J 1998 *J. Phys.: Condens. Matter* **10** 4785
[6] Pendry J B, Holden A J, Robbins D J and Stewart W J 1999 *IEEE Trans. Microwave Theory Tech.* **47** 2075
[7] Shelby R A, Smith D R and Schultz S 2001 *Science* **292** 77
[8] Parazzoli C G, Greegor R B, Li K, Koltenbah B E C and Tanielian M 2003 *Phys. Rev. Lett.* **90** 107401
[9] Grbic A and Eleftheriades G V 2004 *Phys. Rev. Lett.* **92** 117403
[10] Fang N, Lee H, Sun C and Zhang X 2005 *Science* **308** 534
[11] Blaikie R J and Melville D O S 2005 *J. Opt. A: Pure Appl. Opt.* **7** S176
[12] Melville D O S and Blaikie R J 2005 *Opt. Express* **13** 2127
[13] Wiltshire M C K, Hajnal J V, Pendry J B, Edwards D J and Stevens C J 2003 *Opt. Express* **11** 709
[14] Wiltshire M C K, Pendry J B, Young I R, Larkman D J, Gilderdale D J and Hajnal J V 2001 *Science* **291** 849

[15] Wiltshire M C K, Hajnal J V, Pendry J B and Edwards D J 2004 *27th ESA Antenna Technology Workshop on Innovative Periodic Antennas: Electromagnetic Bandgap, Left-handed Materials, Fractal and Frequency Selective Surfaces (Santiago de Compostela, Spain, March 2004)* pp 31–7
[16] Balmain K G 1964 *IEEE Trans. Antennas Propag.* **12** 605
[17] Balmain K G, Luttgen A A E and Kremer P C 2002 *IEEE Antennas Wireless Propag. Lett.* **1** 146
[18] Pendry J B and Ramakrishna S A 2002 *J. Phys.: Condens. Matter* **14** 8463
[19] Ramakrishna S A 2005 *Rep. Prog. Phys.* **68** 449
[20] Smith D R, Schurig D, Rosenbluth M, Schultz S, Ramakrishna S A and Pendry J B 2003 *Appl. Phys. Lett.* **82** 1506
[21] CST GmbH, Darmstadt, Germany
[22] Lagarkov A N and Kissel V N 2004 *Phys. Rev. Lett.* **92** 077401